Vibronic coupling in the icosahedral C_{60}^{2+} Jahn-Teller cation: Repercussions of the nonsimple reducibility of the $H \otimes H$ product

Ian D. Hands, Janette L. Dunn,* Wajood A. Diery,† and Colin A. Bates
School of Physics and Astronomy, University of Nottingham, University Park, Nottingham, NG7 2RD, UK
(Received 21 December 2005; published 30 March 2006)

Coulomb coupling between the two holes in the fullerene cation C_{60}^{2+} results in high- and low-spin terms. Vibronic coupling of the high-spin terms to a single mode of vibration of h_g symmetry can distort the lowest adiabatic potential-energy surface into wells of D_{3d}, D_{5d}, D_{2h}, or C_{2h} symmetry depending upon the precise nature of the coupling produced by different admixtures of the two sets of coupling coefficients arising from the two H-type irreducible representations appearing in the symmetric part of the $H \otimes H$ Kronecker product. The symmetry of dynamic distortions of C_{60}^{2+} ions when coupling to all eight of the possible h_g modes is taken into account depends very closely on both the vibronic coupling parameters and the splittings between different Coulomb terms. Using estimates for these parameters from the literature leads us to conclude that the distortional symmetry is most likely to be D_{2h}, but there is also the possibility that it could be D_{3d}.

DOI: 10.1103/PhysRevB.73.115435 PACS number(s): 61.48.+c, 31.30.Gs

I. INTRODUCTION

In recent years there has been an explosion of research into fullerenes and related materials. However, hole-doped fullerenes have received very little attention in relation to their electron-doped counterparts. Although they are difficult to fabricate experimentally, they, nevertheless, have the potential to exhibit various interesting properties. In particular, it has been predicted that solids containing C_{60} cations could be superconducting at higher temperatures than electron-doped C_{60}.[1–3] One possible reason for this is the nature of the Jahn-Teller (JT) effect in the C_{60} cations. The JT effects in these systems are interesting because the icosahedral symmetry results in high electronic and vibrational degeneracies,[4] with additional complications arising due to the nonsimple reducibility of the H representation.[5,6]

In this paper, we will concentrate on JT effects in the C_{60}^{2+} cation, in which coupling between the two holes of H_u symmetry to eight vibrational modes of h_g symmetry is taken into account. The holes also couple to two a_g modes and six g_g modes, but it has been shown that these modes do not result in any significant distortions[7] so they will not be considered here. We will determine the symmetry of dynamical distortions of a C_{60}^{2+} cation as a function of the vibronic coupling constants and splittings between the Coulomb terms arising from the two holes. It is important to know the symmetry of this distortion as it determines the nature of the vibronic states, which in turn affects the results of experimental (and in particular spectroscopic) observations on these ions.

The dynamical behavior of a JT system can be determined by analyzing the lowest adiabatic potential-energy surface (APES). For C_{60} anions, the APES can contain either ten minima of D_{3d} symmetry, six minima of D_{5d} symmetry, or a trough of equivalent minimum-energy points, depending upon the values of the JT coupling constants.[4] For C_{60} cations, 15 minima of D_{2h} symmetry or 30 minima of C_{2h} symmetry are possible in addition to D_{3d} and D_{5d} minima.[8,9] Using JT coupling parameters calculated for C_{60}^{2+},[7] the overall symmetry of JT distortions of the C_{60}^{2+} ion has previously been calculated to be D_{2h}.[8] In this paper, we will confirm that the distortional symmetry is most likely D_{2h}. However, the symmetry depends closely on the values taken for both the JT coupling parameters and the term splittings, and a small change in the parameter values could result in a symmetry of D_{3d}.

II. HAMILTONIAN

Coulomb interactions between the two holes in the C_{60}^{2+} cation result in allowed terms ^1A_g, ^1G_g, $2\times{}^1H_g$, $^3T_{1g}$, $^3T_{2g}$, and ^3G_g. Calculations indicate that the high-spin terms have energies lower than the low-spin terms.[10,5] As there is no coupling between terms having different spins, we shall consider only the high-spin terms. The JT Hamiltonian describing coupling to a single h_g mode of vibration can thus be written as

$$\mathcal{H}_{JT} = \frac{1}{2}\sum_i \left(\frac{1}{\mu}P_i^2 + \mu\omega^2 Q_i^2\right) + V(H_a \sin\beta + H_b \cos\beta), \tag{1}$$

where the Q_i are the collective coordinates of the h_g mode, the P_i are the conjugate momenta, μ is the reduced mass of the mode, ω is the frequency, and i is summed over the five components $\{\theta, \epsilon, x, y, z\}$ of the h_g mode. H_a and H_b are 10×10 interaction matrices (in the $\{T_1, T_2, G\}$ electronic basis) corresponding to the two sets of Clebsch-Gordan coefficients a and b in Ref. 11 arising from the nonsimple reducibility of the product $H \otimes H$. V is the vibronic coupling constant and the angle β allows for mixing of the two sets of coefficients. The Hamiltonian for the C_{60}^{2+} ion will therefore be written as

$$\mathcal{H} = \sum_{j=1}^{8} \mathcal{H}_{JT}^j + \mathcal{H}_{term}, \tag{2}$$

where $\mathcal{H}_{JT}^j$ is the JT Hamiltonian for mode j and $\mathcal{H}_{term}$ represents the term splittings. We model the latter in terms of a

TABLE I. Conditions to generate minima of a given symmetry (in addition to the condition $Q_x=Q_y=0$). Column 2 gives the general conditions to generate a minimum for arbitrary angle β, while the third column gives the additional conditions for a global minimum of the given symmetry (with the coordinates in units of $\frac{V}{\mu\omega^2}$).

Symmetry	Conditions for minimum	
	at angle β	overall
D_{5d}	$Q_\epsilon=-\sqrt{\frac{2}{3}}Q_z$, $Q_\theta=0$	$\tan\beta=\sqrt{5}$, $Q_z=\frac{3\sqrt{2}}{5}$
D_{3d}	$Q_\theta=-\sqrt{2}Q_z$, $Q_\epsilon=0$	$\tan\beta=\sqrt{\frac{3}{7}}$, $Q_z=-\sqrt{\frac{2}{5}}$
D_{2h}	$Q_z=0$	

diagonal matrix which places the T_{2g} and G_g states at energies δ_1 and δ_2, respectively, above the T_{1g} states. As the energies in this problem depend on the factor $E=V^2/\mu\omega^2$, it is useful to define the dimensionless parameters $\delta_i'=\delta_i/E$ $(i=1,2)$.

III. STRUCTURE OF THE APES

A. Results neglecting Coulomb term splittings

A great deal of information about the behavior of a JT system can be found by analyzing the structure of the lowest-energy APES. As the APES for the C_{60}^{2+} ion is 40-dimensional (eight modes each with five components), we will begin by looking at a single h_g mode with a general coupling constant V and mixing angle β. The positions of the minima in the APES can be found by varying the coordinates Q_i to minimize the lowest eigenvalue of $\mathcal{H}$ for any given values of the angle β and term splittings δ_1' and δ_2'. The symmetry of these points can then be determined by examining the effect of the various symmetry operations of the icosahedral group I_h on these points. This confirms that the minima are either of D_{5d}, D_{3d}, D_{2h}, or C_{2h} symmetry.[8,9] In order to understand the relationships between the different symmetries, it is useful to calculate the minimum energy possible for each symmetry as a function of β. It can be shown that (at least) one point of each symmetry can be generated by considering the coordinates Q_θ, Q_ϵ, and Q_z only (with $Q_x=Q_y=0$). Extra conditions that result in minima of D_{5d}, D_{3d}, and D_{2h} symmetries are given in Table I. As C_{2h} is a subgroup of all of the other three symmetries, the general C_{2h} point also encompasses the other symmetries.

At any given angle β, specific values can be found for the coordinates defining the minimum of any given symmetry. The coordinates of D_{5d} and D_{3d} minima can be found with a one-dimensional (1D) minimization, D_{2h} points with a 2D minimization, and C_{2h} points with a 3D minimization. For example, the lowest D_{2h} point at $\beta=0$ has $Q_\theta=0$ and $Q_\epsilon=\frac{3\sqrt{2}}{4}\frac{V}{\mu\omega^2}$. As β changes from zero, Q_θ becomes nonzero and the value of Q_ϵ reduces. Analytical results can be found for some specific points of interest. For example, the angles β that result in the lowest energies possible for points of D_{5d} and D_{3d} symmetries are given in Table I, along with the corresponding conditions on the coordinates.

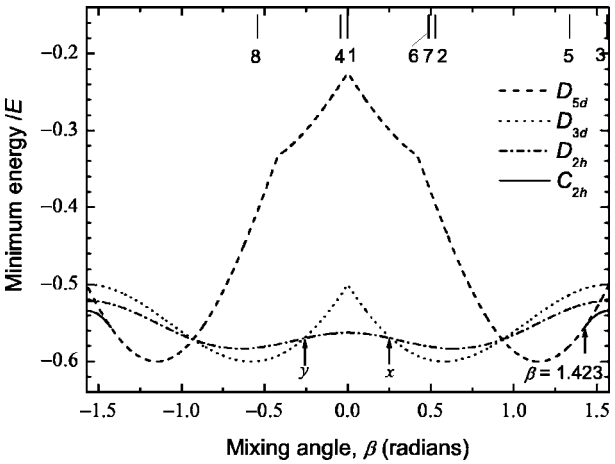

FIG. 1. The variation of the minimum energy obtainable for D_{5d}, D_{3d}, D_{2h}, and C_{2h} symmetries as a function of β in the absence of any term splittings. The bars (|) indicate the calculated mixing angles for the eight h_g modes of C_{60} from Ref. 7.

A plot of the minimum energy obtainable for each symmetry as a function of β is shown in Fig. 1. Results for β outside the range $-\pi/2\leqslant\beta\leqslant\pi/2$ can be obtained by noting that the results repeat if β is changed by π. As C_{2h} is a subgroup of the other three symmetry groups, the curve for C_{2h} is only shown for the region in which the overall symmetry is C_{2h}. It is difficult to determine the value of β at which the crossover to D_{5d} occurs from the energy, but this is easily determined by examining the coordinates. The value is indicated in Fig. 1. It can also be seen that the results are symmetric about $\beta=0$, which is not obvious from the Hamiltonian. The results show that for small values of β, the lowest-energy minima are of D_{2h} symmetry, but as the magnitude of β increases the global minima become first D_{3d}, then D_{5d}, and finally C_{2h} as $|\beta|$ approaches $\pi/2$. Note that at $\beta\approx\pm0.932$ the energies of all of the different symmetries coincide.

Before results can be obtained for a real C_{60}^{2+} ion, it will be necessary to consider both the term splittings and the full multimode problem. However, it is still useful at this stage to look at the effect of the JT coupling on each mode. Table II gives values for the JT coupling constants E and the mixing angles β for the modes $h_g(1)-h_g(8)$ of C_{60} taken from Ref. 7 (using the relationship $E=\frac{1}{4}g^2\hbar\omega$ to convert from their coupling constant g). The angles are also indicated in Fig. 1. Columns A in the table give the minimum energies for each of the modes (which are usually known as the JT energies E_{JT}) along with the predicted symmetry. This shows that $h_g(1)$, which is the most dominant mode, will result in dynamical distortions of D_{2h} symmetry. D_{5d}, D_{3d}, and C_{2h} symmetries are all possible for other modes.

One notable feature of the D_{3d} and D_{5d} curves is that they contain cusps. From Table I, it can be seen that the minimum-energy points for these two symmetries each involve variation along a specific direction in Q space [namely $\mathbf{Q}^{(0)}=\left(0,-\frac{2\sqrt{3}}{5},0,0,\frac{3\sqrt{2}}{5}\right)V/\mu\omega^2$ and $\mathbf{Q}^{(0)}=\left(\frac{2}{\sqrt{5}},0,0,0,-\sqrt{\frac{2}{5}}\right)V/\mu\omega^2$, respectively, for the points identified in Table I]. This allows us to investigate the origin of

TABLE II. The first two columns give the coupling parameters $E\left(\equiv V^2/\mu\omega^2 \equiv \frac{1}{4}g^2\hbar\omega\right)$ and β taken from Ref. 7. The remaining columns give the energy and symmetry of the lowest-energy wells predicted treating each of the eight h_g modes of C_{60}^{2+} separately and including all modes. Columns A give results neglecting term splittings, and B–F give results including term splittings taken from the literature. See text for details. The values of δ_1 and δ_2 for each of the cases are given immediately below the letters A–F. Predicted symmetries which differ from the most commonly predicted symmetry are marked in bold. All of the energies and term splittings are in meV.

Mode	E	β	Well energy and symmetry											
			A (0,0)		B (29,26)		C (−29,−3)		D (6.9,12.4)		E (−6.9,5.5)		F (0,48)	
$h_g(1)$	74.86	−0.0017	−42.2	D_{2h}	−26.9	D_{2h}	−56.0	D_{2h}	−35.5	D_{2h}	−42.3	D_{2h}	−26.6	D_{2h}
$h_g(2)$	19.89	0.525	−11.9	D_{3d}	−7.8	D_{3d}	−29.1	D_{3d}	−9.7	D_{3d}	−10.6	D_{3d}	−7.9	$\boldsymbol{D_{5d}}$
$h_g(3)$	22.03	1.560	−11.8	$\boldsymbol{C_{2h}}$	−7.5	D_{5d}	−36.3	D_{5d}	−9.9	D_{5d}	−16.6	D_{5d}	−11.6	$\boldsymbol{C_{2h}}$
$h_g(4)$	14.96	−0.040	−8.4	$\boldsymbol{D_{2h}}$	−2.2	D_{3d}	−31.7	D_{3d}	−3.5	D_{3d}	−11.0	D_{3d}	−2.2	D_{3d}
$h_g(5)$	1.69	1.337	−1.0	D_{5d}	−0.4	D_{5d}	−29.2	D_{5d}	−0.5	D_{5d}	−7.2	D_{5d}	−1.0	D_{5d}
$h_g(6)$	10.65	0.488	−6.4	D_{3d}	−3.4	D_{3d}	−29.1	D_{3d}	−4.2	D_{3d}	−7.1	$\boldsymbol{D_{5d}}$	−4.0	$\boldsymbol{D_{5d}}$
$h_g(7)$	41.77	0.490	−25.1	D_{3d}	−19.4	D_{3d}	−29.9	$\boldsymbol{D_{2h}}$	−21.9	D_{3d}	−23.6	D_{3d}	−16.7	D_{3d}
$h_g(8)$	37.17	−0.543	−22.3	D_{3d}	−0.2	D_{3d}	−46.2	D_{3d}	−14.1	D_{3d}	−26.3	D_{3d}	−15.0	$\boldsymbol{D_{5d}}$
Total			−99.3	D_{2h}	−85.3	$\boldsymbol{D_{3d}}$	−108.5	D_{2h}	−93.3	D_{2h}	−98.7	D_{2h}	−82.2	D_{2h}

these cusps by writing the coordinates of the minimum-energy point at a given angle β in terms of a coefficient c multiplying the coordinates $\mathbf{Q}^{(0)}$. Figure 2 shows the value of c required to produce the lowest energy possible for each angle β. This shows that the cusps in the energies are mirrored by cusps or discontinuities in the coordinates of the minimum-energy points. The discontinuities correspond to changes in the sign of the coefficient c, showing that there is a competition between possible minima in the directions $+\mathbf{Q}^{(0)}$ and $-\mathbf{Q}^{(0)}$.

B. Separation of minima

Minima of a given symmetry are equivalent in the sense that they all have the same energies. However, they are not all equally separated in Q space. Before moving on to consider the effect of term splittings, we will investigate these geometrical separations. It is useful to determine the numbers of nearest neighbors, next-nearest neighbors, etc., to a given well because the overlap between wave functions in two wells decreases as the separation of the wells increases. Thus tunneling between the wells, as it may be possible to observe in ultrafast optical experiments, for example, becomes less likely.[12]

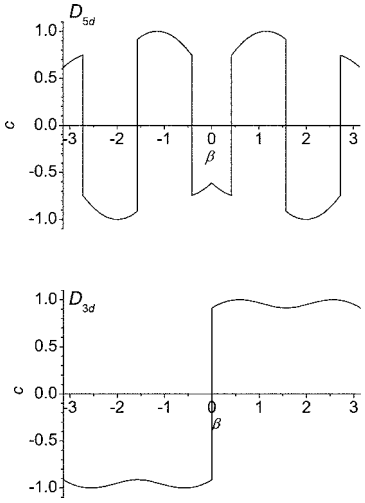

FIG. 2. The variation of the coefficient c multiplying the minimum-energy coordinates for D_{5d} and D_{3d} symmetries as a function of β in the absence of any term splittings.

Taking the conditions for generating a minimum of a chosen symmetry in the $\{Q_\theta, Q_\epsilon, Q_z\}$ plane given in Table I, we can obtain symbolic expressions for the positions of all other wells of that symmetry by applying matrices representing C_2, C_3, and C_5 rotations of the icosahedral group. These can be used to obtain expressions for the distances (in Q space) between the generating well and all other wells of that symmetry. The results for these distances and the number of wells at each of the distances are given in Table III. Obviously, equivalent results would be obtained if a different well was chosen as the starting point, although our choice is particularly convenient as all generating points lie in the $\{Q_\theta, Q_\epsilon, Q_z\}$ plane.

From Table III, it can be seen that each D_{5d} well has five nearest neighbors and each D_{3d} well has three nearest-neighbors and six next-nearest neighbors. A similar pattern has been observed in other icosahedral systems. This is not surprising as our approach only involves taking a general point of the chosen symmetry and applying operators of the icosahedral group; no part of the calculation is specific to the C_{60}^{2+} ion. For the D_{2h} and C_{2h} wells, the determination of nearest neighbors, next-nearest neighbors, etc., is rather more complicated. As the relative separations of different wells depends on the Q_i, which in turn depend on the angle β, the ordering of the wells by distance also depends on β.

Table IV gives the values of the coordinates Q_i of the D_{2h} and C_{2h} wells at selected mixing angles β for which these wells are absolute minima, together with the order of the subsets of wells as defined in Table III. This shows that, over the range of angles for which D_{2h} wells can be absolute

TABLE III. Distances between minima and the number of minima at that distance, in terms of the coordinates Q_i that define a minimum in the $\{Q_\theta, Q_\epsilon, Q_z\}$ plane (as defined in Table I) and with $Q_\pm = \frac{5}{2}Q_\theta^2 \pm \sqrt{3}Q_\theta Q_\epsilon + \frac{3}{2}Q_\epsilon^2$. The results for D_{2h} are ordered in terms of increasing separation over the range for which D_{2h} points can be absolute minima ($-0.25 < \beta < 0.25$) and the results for C_{2h} are ordered in terms of increasing separation for $\beta = \pi/2$.

	Subset	No.	Distance
D_{5d}	1	5	$4Q_z^2$
D_{3d}	1	3	$4Q_z^2$
	2	6	$8Q_z^2$
D_{2h}	1	4	Q_-
	2	4	Q_+
	3	4	$Q_\theta^2 + 3Q_\epsilon^2$
	4	2	$3(Q_\theta^2 + Q_\epsilon^2)$
C_{2h}	1	2	$Q_+ - \sqrt{2}Q_\theta Q_z - \sqrt{6}Q_\epsilon Q_z + Q_z^2$
	2	2	$Q_- + \sqrt{2}Q_\theta Q_z - \sqrt{6}Q_\epsilon Q_z + Q_z^2$
	3	2	$Q_- - \sqrt{2}Q_\theta Q_z + \sqrt{6}Q_\epsilon Q_z + Q_z^2$
	4	2	$Q_\theta^2 + 3Q_\epsilon^2 - 2\sqrt{2}Q_\theta Q_z + 2Q_z^2$
	5	4	$Q_\theta^2 + 3Q_\epsilon^2 + 2Q_z^2$
	6	4	$3(Q_\theta^2 + Q_\epsilon^2) + 2Q_z^2$
	7	2	$Q_+ + \sqrt{2}Q_\theta Q_z + \sqrt{6}Q_\epsilon Q_z + Q_z^2$
	8	2	$Q_\theta^2 + 3Q_\epsilon^2 + 2\sqrt{2}Q_\theta Q_z + 2Q_z^2$
	9	4	$Q_- + 3Q_z^2$
	10	4	$Q_+ + 3Q_z^2$
	11	1	$4Q_z^2$

minima, the pattern of well separations from nearest to furthest neighbors is 4,4,4,2. Our result is a generalization of that obtained in Ref. 8 using parameters specifically for the C_{60}^{2+} ion. Further calculations show that the same pattern is obtained for all values of β, although the subsets containing four wells do interchange.

The pattern is particularly complicated for the C_{2h} wells, where there are 11 different subsets of wells. Table IV shows that the pattern of separations for $\beta = \pm 1.50$ is 2,2,2,2,4,4,2,2,4,4,1 but when β is reduced slightly to ± 1.45, two pairs of sets interchange and the pattern becomes 2,2,2,2,4,4,2,4,2,4,1. It is interesting to note that the pattern of four subsets of four wells, six subsets of two wells, and a single well is the same as that obtained in Ref. 8 for the low-spin states of both C_{60}^{2+} and C_{60}^{5+} (albeit in different orders), and is similar to that for spin 1 state of C_{60}^{4+} except that in this latter case a set of four wells and a set of two wells are at equivalent distances. This confirms that the pattern of neighbors is a property of C_{2h} wells within the icosahedral group and is not specific to C_{60}^{2+} ions.

C. Effect of Coulomb term splittings

We will now consider the effect of the term splittings on the single-mode results. We will begin by choosing values that illustrate the effects of these contributions, before moving on to consider values appropriate to the C_{60}^{2+} ion. Results for $\delta_1' = 0.2$ and $\delta_2' = 0$ are shown in Fig. 3, and those for $\delta_1' = 0$ and $\delta_2' = 0.2$ in Fig. 4. The most obvious feature is that the energies are no longer symmetric about $\beta = 0$ in Fig. 3 (although they do still repeat when β is changed by π), but they are still symmetric in Fig. 4. It can be shown analytically that for nonzero δ_2', the energy for negative β is related to that for positive β in exactly the same way as that obtained in the absence of term splitting. However, this is not the case for nonzero δ_1'.

TABLE IV. Coordinates, in units $\frac{V}{\mu\omega^2}$, of one of the D_{2h} and one of the C_{2h} wells in the $\{Q_\theta, Q_\epsilon, Q_z\}$ plane at selected mixing angles β for which the points are absolute minima. Also given is the ordering, in terms of increasing separation, of the different subsets of wells as defined in Table III. Note that for $\beta = 0$, the wells numbered 3 and 4 are equidistant from the reference well, as are wells numbered 1 and 2.

β	Q_θ	Q_ϵ	Q_z	Order
D_{2h}				
−0.25	0.156	1.056		1,2,3,4
−0.15	0.092	1.059		1,2,3,4
−0.05	0.031	1.061		1,2,3,4
0	0	1.061		{1,2}, {3,4}
0.05	−0.031	1.061		2,1,3,4
0.15	−0.092	1.059		2,1,3,4
0.25	−0.156	1.056		2,1,3,4
C_{2h}				
1.5	0.281	−0.240	−0.970	1,2,3,4,5,6,7,8,9,10,11
1.45	−0.193	−0.446	−0.928	1,2,4,3,5,6,7,9,8,10,11
−1.45	0.193	−0.446	−0.928	2,1,8,7,5,6,3,10,4,9,11
−1.5	0.281	−0.240	−0.970	2,1,7,8,5,6,3,4,10,9,11

Figure 3 shows that with $\delta_1' = 0.2$, the energies tend to increase in the range $-\frac{\pi}{2} < \beta < 0$ compared to $\delta_1' = 0$, while the results for $0.2 < \beta < 1$ are almost unaffected. If $\delta_1' = -0.2$, the energies appear similar to reflecting those shown in Fig. 3 about $\beta = 0$, except that over the range $-\frac{\pi}{2} < \beta < 0$ the energies are now decreased rather than increased. Results for stronger values of $|\delta_1'|$ continue to emphasize the asymmetry about $\beta = 0$. Figure 4 shows that the

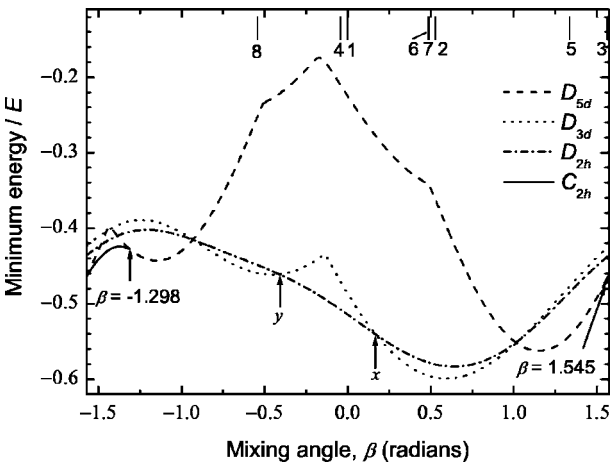

FIG. 3. As Fig. 1 but including a term splitting $\delta_1' = 0.2$.

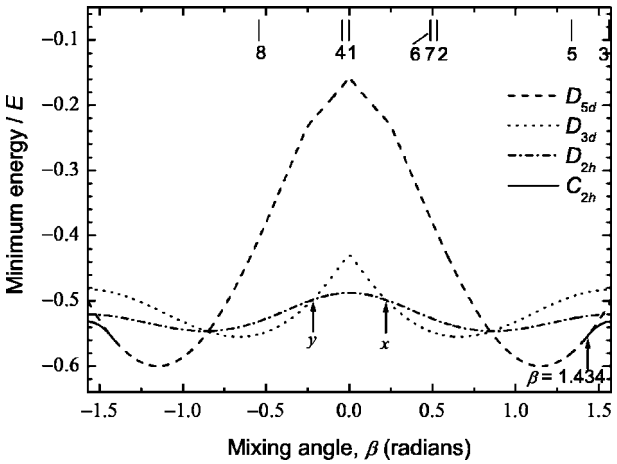

FIG. 4. As Fig. 1 but including a term splitting $\delta_2'=0.2$.

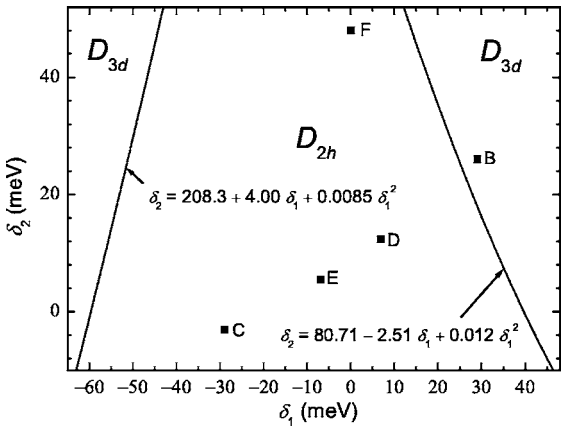

FIG. 5. The regions of D_{2h} and D_{3d} symmetries possible for a C_{60}^{2+} ion as a function of the term splittings, calculated using the coupling constants and frequencies given in Ref. 7, along with approximate equations for the boundaries over the ranges plotted. The marked points (■) correspond to the calculated values of the term splittings extracted from the literature.

energies near $\beta=0$ have been increased compared to the $\delta_2'=0$ results while those near $\beta=\pm\frac{\pi}{2}$ are much less affected. For $\delta_2'=-0.2$, the energies near $\beta=0$ are decreased rather than increased.

It has not yet been possible to determine the multiplet structure of the C_{60}^{2+} ion experimentally,[13] although we can deduce five different theoretical estimates for δ_1 and δ_2 from the literature, noting that difficulties in assigning symmetry labels to the T_1 and T_2 states leads to ambiguity in their ordering. Referring to the case without term splittings as A, the other cases are as follows:

B: $(\delta_1,\delta_2)=(29,26)$, calculated using a multipole expansion of the Coulomb interactions.[10]

C: $(\delta_1,\delta_2)=(-29,-3)$, a modification of B arising from interchange of the T_1 and T_2 labels.[14,15]

D: $(\delta_1,\delta_2)=(6.9,12.4)$, from a self-consistent field method,[13] assuming T_1 is below T_2.

E: $(\delta_1,\delta_2)=(-6.9,5.5)$, as in D but assuming that T_1 is above T_2.

F: $(\delta_1,\delta_2)=(0,48)$, obtained using density-functional electronic structure calculations.[16]

The values of E and β from Ref. 7 (as summarized in Table II) allow us to determine the symmetry of dynamic distortions that would be obtained for the C_{60}^{2+} ion if each mode could be considered in isolation. The results are given in Table II. It can be seen that the predicted symmetry for modes 1 and 5 does not depend on the values of the term splitting. This is because the values of β for these modes are a long way from the values at which the symmetry of the lowest-energy curve changes. All of the other modes have two possible symmetries depending upon the choice made for the term splittings.

IV. MULTIMODE CALCULATION

We are now in a position to obtain results for the C_{60}^{2+} ion by minimizing the energy with all eight modes and including the term splittings. The results are contained in Table II, with our conclusions concerning the symmetries summarized in the bottom line. In general, the overall symmetry in a multimode problem will be the same as that of the most strongly coupled mode. The addition of weaker modes will alter the positions of the minimum-energy wells but will not alter the overall symmetry. In the problem under consideration here, $h_g(1)$ is the most dominant mode and has D_{2h} symmetry, so it would be expected that the overall symmetry will be D_{2h}. This is despite the fact that the lowering of energy involving mode 1 is only between 32% and 52% of the overall lowering obtained when all eight modes are considered. However, this is not the case with the term splittings in case B. In this case, the D_{3d} minima for mode $h_g(1)$ are only slightly higher in energy than the D_{2h} minima. The inclusion of additional modes that predominantly prefer D_{3d} symmetry results in an overall symmetry of D_{3d}. The interplay between the symmetries of the different modes, which is determined by the mixing angles β, means that particular care must be taken if this system is treated in terms of a single effective vibrational mode rather than performing a full multimode calculation.

Figure 5 shows the boundaries between the regions where D_{2h} and D_{3d} are lowest as a function of the term splittings. As $h_g(1)$ is the most strongly coupled mode, the form of the diagram for $\beta=0$ in the single-mode case has a qualitatively similar form to that of Fig. 5, which allows us to interpret the form of the multimode results. Figure 3 shows that, if δ_1 is increased from zero and δ_2 kept constant, the point x at which the D_{2h} and D_{3d} symmetries cross moves towards lower values of β. There will therefore be a value of δ_1 at which x moves through $\beta=0$, signalling a change in symmetry. Similarly, as δ_1 is decreased below zero, the crossover point y moves towards $\beta=0$ until another crossover occurs. Figure 4 shows that as δ_2 is increased, the region between x and y for which D_{2h} is lowest, is reduced. Thus increasingly smaller magnitudes of δ_1 are needed to generate a crossover as δ_2 is increased.

V. DISCUSSION

This paper has sought to bring a greater understanding to the interplay between the different symmetries involved in

the JT problem of two holes coupled to an h_g mode in icosahedral symmetry, the effect of Coulomb term splittings on these results, and the extension of these results to the C_{60}^{2+} ion coupled to eight h_g modes.

Manini and co-workers[8,9] using results from their earlier *ab initio* density-functional calculations for the single-hole vibronic coupling constants,[7] predicted that the minima in the lowest APES for C_{60}^{2+} will be of D_{2h} symmetry. Our results confirm that the symmetry is D_{2h} for the coupling parameters, mixing angles, vibrational frequencies, and term splittings reported in the literature. However, we have shown that the symmetry is very dependant upon these parameter values. Values for the term splittings implied in Ref. 7 are quite different to those obtainable from other papers in the literature. Hence it was not at all obvious that calculations using these different term splittings would also result in a prediction of D_{2h} symmetry.

It should be further noted that only one set of estimates of the JT parameters is available in the literature. Any new calculations could have a strong effect on the overall symmetry predicted, particularly if the mixing angle for the $h_g(1)$ mode is revised. Our results give a clear indication of how the predicted distortional symmetry of C_{60}^{2+} ions will change if estimates of the parameters are revised in the future. Finally, it should be noted that no numerical values for the JT and Coulomb parameters have been obtained experimentally. Although the *ab initio* calculations have provided some insight, determination should also be sought experimentally. This is particularly true of the mixing angles, which are not possible to determine on symmetry grounds alone.

In this paper, we have sought to provide a clear picture of the complicated structure of the APES in the JT problem applicable to C_{60}^{2+} ions. However, this is only part of the complete picture needed to understand the dynamical behavior of these ions. In particular, while the energies given in Table II are useful in that they give an indication of the contribution of each of the eight h_g modes to the overall problem, they do not represent the energies of the system as a whole. The APES defines the underlying potential through which the system will move. If the JT coupling is strong compared to the vibrational quanta $\hbar\omega_i$ for each of the eight modes i (which can be found from the literature), the states of the system could be expected to be harmonic oscillator-type states associated with the lowest-energy wells in the APES. However, as in all JT systems, the vibronic coupling will alter the curvature of the wells and introduce anisotropy, such that the frequency of each component i of any of the h_g modes will no longer be simply ω but a new frequency ω_i that is in general smaller than ω due to broadening of the well.[8] The size of this mode softening can be calculated using the Hessian matrix of second-order derivatives of the potential.[8,17] The energy of the ground state of a system coupled to a single mode will therefore be approximately $\Sigma_i \frac{1}{2}\hbar\omega_i$ higher than the well energies given in Table II. Estimates of the coupling constants and frequencies indicate that the vibronic coupling is not sufficiently strong in C_{60}^{2+} ions to consider well states alone. States of the system will be linear combinations of the states associated with the wells, which physically represent tunneling between the wells.[18] Generally, this will result in raising the energy of the ground state above the value obtained after applying the zero-point corrections. While such states (and their energies) can be determined, using projection operators, for example,[18,19] this is beyond the scope of this paper and should form the basis of future work.

ACKNOWLEDGMENTS

We would like to thank EPSRC for funding this work. We also wish to thank A. Nikolaev and B. N. Plakhutin for communications involving their term splitting calculations, and N. Manini for useful discussions.

*Author to whom correspondence should be addressed. Electronic address: janette.dunn@nottingham.ac.uk; URL: http://www.nottingham.ac.uk/~ppzjld

†Present address: Department of Physics, King Abdulaziz University, Jeddah, Saudi Arabia.

[1] M. Granath and S. Östlund, Phys. Rev. B **66**, 180501(R) (2002).

[2] A. M. Panich, I. Felner, A. I. Shames, S. Goren, P. K. Ummat, and W. R. Datars, Solid State Commun. **129**, 81 (2004).

[3] P. Paci, E. Cappelluti, C. Grimaldi, L. Pietronero, and S. Strassler, Phys. Rev. B **69**, 024507 (2004).

[4] C. C. Chancey and M. C. M. O'Brien, *The Jahn-Teller Effect in C_{60} and Other Icosahedral Complexes* (Princeton University Press, Princeton, NJ, 1997).

[5] N. Manini and P. De Los Rios, Phys. Rev. B **62**, 29 (2000).

[6] E. Lijnen and A. Ceulemans, Phys. Rev. B **71**, 014305 (2005).

[7] N. Manini, A. Dal Corso, M. Fabrizio, and E. Tosatti, Philos. Mag. B **81**, 793 (2001).

[8] M. Lüders, N. Manini, P. Gattari, and E. Tosatti, Eur. Phys. J. B **35**, 57 (2003).

[9] M. Lüders and N. Manini, Adv. Quantum Chem. **44**, 289 (2003).

[10] A. V. Nikolaev and K. H. Michel, J. Chem. Phys. **117**, 4761 (2002).

[11] P. W. Fowler and A. Ceulemans, Mol. Phys. **54**, 767 (1985).

[12] I. D. Hands, J. L. Dunn, and C. A. Bates, Phys. Rev. B **73**, 014303 (2006).

[13] M. Wierzbowska, M. Luders, and E. Tosatti, J. Phys. B **37**, 2685 (2004).

[14] B. N. Plakhutin, J. Chem. Phys. **119**, 11429 (2003).

[15] A. V. Nikolaev and K. H. Michel, J. Chem. Phys. **120**, 8334 (2004).

[16] M. Lüders, A. Bordoni, N. Manini, A. Dal Corsa, M. Fabrizio, and E. Tosatti, Philos. Mag. B **82**, 1611 (2002).

[17] Y. M. Liu, J. L. Dunn, C. A. Bates, and V. Z. Polinger, J. Phys.: Condens. Matter **9**, 7119 (1997).

[18] J. L. Dunn and C. A. Bates, Phys. Rev. B **52**, 5996 (1995).

[19] L. D. Hallam, C. A. Bates, and J. L. Dunn, J. Phys.: Condens. Matter **4**, 6775 (1992).